Available online at www.sciencedirect.com

SciVerse ScienceDirect

Scripta Materialia 68 (2013) 207–210

Scripta MATERIALIA

www.elsevier.com/locate/scriptamat

Pre-straining effects on the power-law scaling of size-dependent strengthening in Ni single crystals

Jaafar A. El-Awady,[a,*] Michael D. Uchic,[b] Paul A. Shade,[b] Sang-Lan Kim,[c] Satish I. Rao,[c] Dennis M. Dimiduk[b] and Christopher Woodward[b]

[a] *Department of Mechanical Engineering, Johns Hopkins University, Baltimore, MD, USA*
[b] *Air Force Research Laboratory, Wright-Patterson AFB, OH, USA*
[c] *UES Inc., Dayton, OH, USA*

Received 8 February 2012; revised 20 October 2012; accepted 20 October 2012
Available online 27 October 2012

We report experimental and three-dimensional discrete dislocation dynamics measurements to characterize the effect of high starting dislocation density on size-affected flow. Microcrystals were focused ion beam milled into a pre-strained bulk Ni single crystal to obtain a dense heterogeneous dislocation cell structure. The strength-scaling exponent is shown to decreases considerably with increasing dislocation density. Cutting the pre-existing forest during microcrystal fabrication can lead to alternate pathways for the advancing slipped areas to defeat the forest, resulting in a lower strength than the pre-strained bulk crystal.

Keywords: Dislocation density; Size effects; Pre-straining; Nickel microcrystals; Discrete dislocation dynamics

Extrinsic size effects in metals and alloys have been a rich topic of research over the past decade, and continues to grow with numerous new challenges and questions emerging at the micro- and nanoscales. Interest in these topics was sparked by the first compression experiments on microcrystals fabricated from bulk crystals using the focused ion beam (FIB) technique [1,2]. These early results showed a complete deviation from bulk-like behavior and clear size-dependent strengthening, with smaller crystals significantly stronger than larger crystals. This characteristic behavior was shown to be persistent in many different materials and under different loading conditions [3,4]. In addition, the relationship between strength and microcrystal diameter, D, follows a power-law relationship with an exponent that is typically in the range of -0.2 to -1.0 [3,4].

Recently, attention has been directed towards investigating the influence of the pre-existing dislocation density on the strength-scaling exponent. In this regard, one of the earliest experimental studies was performed on defect-free directionally solidified Mo-alloy microcrystals grown in an NiAl matrix [5,6]. All compressed microcrystals having sizes $0.36 \leqslant D \leqslant 1.0$ μm yielded near their theoretical shear strength and no size effects were observed. On the other hand, by first pre-straining the parent material to 4% strain, the strength of the tested microcrystals dropped significantly and a clear size effect was observed. Furthermore, by first pre-straining the parent material to 11% strain, all tested microcrystals were observed to deform in a bulk-like manner, with no observed size effects [6]. Due to the small Mo fiber sizes in the bulk crystal, dislocation arrangement introduced by bulk pre-straining was random and no well-defined dislocation cell structure was observed.

Sub-micron Au pillars FIB milled from high- and low-aspect-ratio pre-strained microcrystals also showed a dramatic decrease in flow strength with increasing pre-strain [7]. Contrary to those results, Schneider et al. [8] showed that microcrystals FIB milled from pre-strained Mo microcrystals with diameters between 0.3 and 5.0 μm exhibit no change in strength. Thus, further experimental analysis is necessary to explain such conflicting observations. In conjunction with these experimental studies, the first systematic computational study to evaluate the effect of the initial dislocation density on the strength-scaling exponent was made utilizing three-dimensional discrete dislocation dynamics (DDD) simulations [9]. From these simulations it was shown that the strength-scaling exponent varies from -0.84

* Corresponding author. Tel.: +1 410 516 6683; e-mail: jelawady@jhu.edu

1359-6462/$ - see front matter © 2012 Acta Materialia Inc. Published by Elsevier Ltd. All rights reserved.
http://dx.doi.org/10.1016/j.scriptamat.2012.10.035

at a low initial dislocation density of 7×10^{11} m^{-2} to -0.43 at an initial dislocation density of 10^{13} m^{-2}.

In this study we evaluate the effect of an existing heterogeneous dislocation cell structure on the size-affected flow response. A large 99.999% pure nickel single crystal grown by the Bridgman technique was purchased from Goodfellow Corporation, USA. The crystal had a cylindrical geometry, with diameter $D = 20$ mm and length $L = 79$ mm. The crystal orientation was determined using Laue X-ray diffraction to be parallel to the [0 0 1] direction within $\pm 2°$. A rectangular specimen was then cut from the large crystal by wire electrical discharge machining (EDM), with its long edges being parallel to the [1 1 0] direction. The lateral faces were oriented such that the surface normals corresponded to the [0 0 1] and [1 $\bar{1}$ 0] directions. The dimensions of the parent crystal were $3.3 \times 3.3 \times 9.0$ mm^3 (aspect ratio of 2.73). To insure the removal of any altered microstructure that may have developed in the surface layer during the EDM process, all surfaces of the specimen were mechanically polished to a 6 μm finish. This was followed by electrolytic polishing to further remove an addition 30 μm layer from the surface. Finally, the specimen was thermally annealed at 1365 °C for 336 h in a purified argon environment at a back pressure of 1 psi. Immediately after annealing, a single measurement of the initial dislocation density was made using the etch pitting technique [10]. This measurement indicated an initial dislocation density of 2.5×10^8 m^{-2}. The etch pit method estimates a dislocation density that is typically 1.5 times lower than the actual dislocation density in the crystal [11]. Allowing for this correction, the true dislocation density in these crystals would be $\approx 3.75 \times 10^8$ m^{-2}.

The specimen was pre-deformed under uniaxial compression to 23% engineering strain in a Sintech 20/G testing machine (MTS/Sintech, Research Triangle Park, NC). Testing was performed at room temperature and at a constant nominal applied strain rate of $\approx 1 \times 10^{-5}$ s^{-1}. Deformation along the [1 1 0] crystallographic orientation is stable against lattice rotations, and produces the simultaneous activation of dislocations on two slip planes: [0 $\bar{1}$ 1](1 1 1), [$\bar{1}$ 0 1](1 1 1), [0 1 1](1 $\bar{1}$ 1) and [1 0 1](1 $\bar{1}$ 1). The Schmid Factor (SF) for these four slip systems is 0.41, and 0 on all other slip systems. The engineering stress reached at the end of the experiment was 384.5 MPa. Using the Taylor hardening relation, this suggests a dislocation density of 4×10^{14} m^{-2} at the end of pre-deformation. The onset of stage III is observed to be $\tau_{III} = 77 \pm 7$ MPa, which is in agreement with previously reported values for Ni single crystals (e.g. [12]).

Figure 1(a) shows the dislocation substructure at the end of pre-deformation via scanning transmixxion electron microscopy (STEM) imaging. The foil plane is (1 1 0), which coincides with the orientation of the microcrystals fabricated from this specimen for subsequent testing. Dislocations are arranged in cellular structures having a mean cell size on the order of 0.5 to 1.0 μm, which is also indicative of the stage III microstructure in face-centered cubic (fcc) metals [12].

After pre-deformation, a thin slice having a [1 1 0] orientation was cut by EDM from the center of the pre-strained specimen (parent crystal). The surfaces of this slice were then electrolytically polished to remove any altered structure resulting from the EDM process. Several

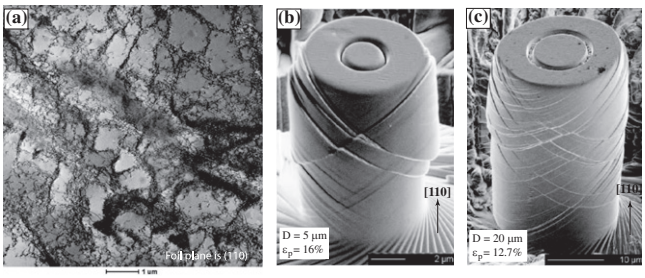

Figure 1. (a) Dislocation microstructure as observed by bright-field STEM at the center of the 23% strained bulk specimen (parent crystal). (b) SEM image of a child microcrystal having $D = 5$ μm after 16% strain. (c) SEM image of a child microcrystal having $D = 20$ μm after 12.7% strain.

cylindrical microcrystals (child crystals) having diameters in the range of $2 - 20$ μm were then FIB milled into the slice with a constant aspect ratio of $L{:}D = 2.3$. The axial direction of all fabricated microcrystals was parallel to the [1 1 0]. Microcrystal compression tests were then carried out in a nanoindenter system (MTS Nano XP) with a flat-ended diamond tip [1]. A coupled displacement-controlled and stress-controlled loading technique identical to that described in Ref. [13] was imposed. The nominal applied strain rate was approximately 1×10^{-4} s^{-1}.

Figure 1(b) and (c) shows scanning electron microscopy (SEM) micrographs of two deformed microcrystals having sizes $D = 5.0$ and 20 μm, which were deformed to 16% and 12.7% strain, respectively. As expected for the deformation of [1 1 0] oriented crystals, a symmetric-slip deformation is observed on the two non-zero SF slip planes: (1 1 1) and (1 $\bar{1}$ 1), respectively.

The engineering stress–strain curves for the 23% pre-deformed specimen, alongside the engineering stress–strain curves for the deformed [1 1 0] oriented microcrystals, are shown in Figure 2. A clear size-scale effect is observed, with the flow strength increasing as the microcrystal diameter decreases. Successive strain bursts separated by elastic loadings were also observed after yielding for all microcrystals tested, which was also observed in previous microcrystal studies of Ni at lower initial dislocation density [13,14]. This response is quite distinctive from the response previously reported for 11% pre-strained molybdenum sub-micron pillars [6].

Phani et al. [15] showed that the dislocation density in Mo single-crystal fibers highly pre-strained in an

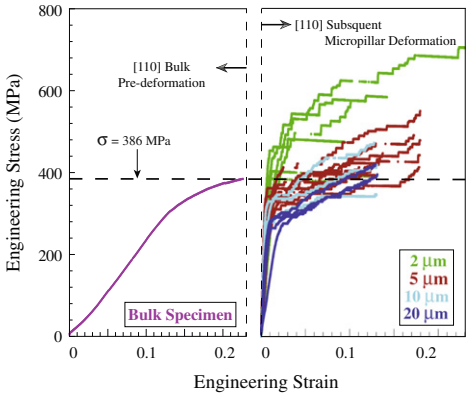

Figure 2. Engineering stress–strain curves of the 23% pre-deformed parent crystal, alongside the [1 1 0] oriented child microcrystals.

NiAl–Mo fibrous composite is high and uniform throughout the Mo fiber. The deformation of Mo microcrystals extracted from these fibers did not show any size effects [6]. In our current study, the pre-strained dislocation density is high but not uniform. The dislocation density is arranged in cell-like structures (see Fig. 1). The average dislocation cell size for the 23% pre-strained specimen is $0.5 - 1.0$ μm. Therefore, the smallest microcrystals tested have roughly 2–4 dislocation cells spanning their diameter.

A unique feature observed from Figure 2 is that the initial flow strength of microcrystals having $D \geqslant 5$ μm is consistently lower than the strength of the parent bulk crystal at the end of pre-straining, $\sigma_{Bulk,\epsilon=23\%} = 386$ MPa. In particular, the flow strength at 4% strain for the $D = 20$ μm microcrystals is ≈20% lower than the strength of the pre-strained parent crystal. In addition, the work-hardening rate for the $D = 20$ μm microcrystals is approximately linear with a coefficient $\theta = 1100^{\pm 100}$ MPa. This is distinctively different from the work-hardening rate of the parent crystal at the end of pre-straining, which is parabolic, with $\theta_{Bulk,\ \epsilon=23\%} = 470$ MPa, or the work-hardening coefficient of stage II (linear hardening stage), with $\theta_{Bulk,stage-II} = 2500$ MPa. Thus, these microcrystals deform in a stage-II fashion, but with a lower flow strength and work-hardening rate than the parent crystal.

The observed softening of the larger microcrystals may be attributed to a number of different effects. The characteristic length of the slipped area (invading finger width) that advances through the forest in a non-planar front is much larger than the point-to-point spacing of hard forest dislocations [16]. In our experiments, fabricating the child crystals results in artificially selecting only a subregion of the dislocation forest and bounding this region with free surfaces, giving the evolving dislocations new pathways to defeat the forest at yield. Thus, these "fingers" may find other pathways to defeat the forest at yield, especially if the free surface is effective at promoting cross-slip [17]. This may be responsible for the observed lower strength of the larger microcrystals tested.

On the other hand, according to the composite model of Mughrabi [18], the heterogeneous dislocation microstructure (i.e. dislocation cell structure) can be treated as a two-phase material, having plastically hard walls and softer interior cells. The flow strength predicted by this model is 25% lower compared to a uniformly distributed dislocation density (i.e. Taylor hardening law). This is in qualitative agreement with our current results on microcrystals with sizes $D = 20$ μm, which might suggest that there is a characteristic length below which the flow strength is dominated by the heterogeneity of the cellular dislocation substructure. Further investigations are needed with microcrystal diameters larger than 20 μm to identify this transition; these "larger" microcrystals could not be prepared in the present study due to the significant quantity of FIB milling time required to fabricate such samples.

Figure 3 shows a log–log plot of the critical resolved shear strength (CRSS) on the primary slip plane vs. microcrystal diameter for the 23% pre-strained crystals. The CRSS is computed at 2% engineering strain due to experimental difficulties in obtaining optimal sample-to-indenter alignment for the entire array of crystals [19]. For comparison, the results for two previous studies of Ni microcrystals tested with a moderate initial dislocation density on the order of 10^{12} m^{-2} are also shown [13,14]. The strength-scaling relationship for these microcrystals was observed to follow a power law with an exponent in the range of -0.64 to -0.69. In comparison, the 23% pre-strained [1 1 0] microcrystals exhibit a power-law scaling exponent of -0.164. The initial dislocation density in the 23% pre-strained microcrystals as evaluated by the Taylor relation is 4×10^{14} m^{-2}, which is two orders of magnitude higher than those reported in [13,14].

To understand the effect of the initial dislocation density on the strength-scaling exponent, we analyzed three-dimensional (3-D) DDD simulations performed on Ni microcrystals having diameters in the range of 0.25–20 μm. The initial dislocation density was varied in the range of 1.0×10^{11}–1.3×10^{13} m^{-2}. The log–log plot of the CRSS at 1% engineering strain vs. microcrystal diameter is shown in Figure 4(a). This is a composite of the simulation results that were performed by some of the current authors and were published previously in Refs. [9,20,21], as well as additional simulations with the same conditions. It should be noted that, due to computational difficulties, these dislocation densities are an order of magnitude lower than those in the current experiments. The initial dislocation distribution in the DDD simulations are based on a random distribution of spiral and Frank–Read sources mimicking those observed in Ref. [15]. It is clear that, similar to experiments, DDD simulations show that an increase in the initial dislocation density is accompanied by a decrease in the power law exponent.

It is also observed that sub-micron pillars exhibit a reduction in flow strength with increasing initial dislocation density. This is in qualitative agreement with pre-strained $D \leqslant 0.5$ μm Au microcrystals, which showed a reduction in flow strength with increasing pre-straining extent [7]. This softening effect due to the increasing initial dislocation density can be explained as follows. A modified Taylor hardening relationship that accounts for the strength required to operate a source as well as overcome forest dislocations can be expressed as: $\tau = \tau_{source} + \tau_{forest} = Gb/\lambda + \alpha Gb\sqrt{\rho}$, where b is the Burgers vector, G is the shear modulus, $\alpha = 0.5$ and λ is the mean

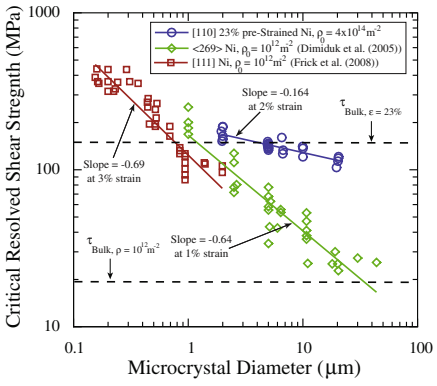

Figure 3. Log–log plot of the CRSS on the primary slip-plane vs. diameter for [1 1 0]-oriented microcrystals FIB milled into the center of a 23% pre-strained bulk [1 1 0] Ni single crystal. For comparison, the results from Refs. [13,14] of microcrystals having a moderate initial dislocation density of 10^{12} m^{-2} and orientations ⟨2 6 9⟩ and [1 1 1], respectively, are shown.

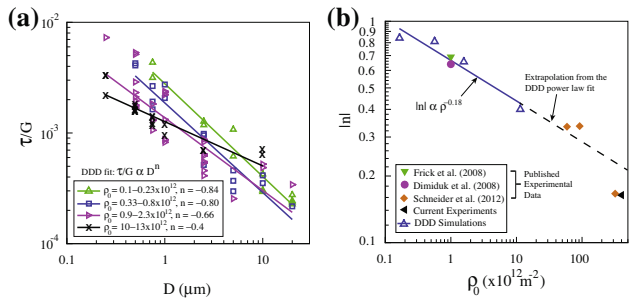

Figure 4. Log–log plots of: (a) CRSS vs. microcrystal diameter from 3-D DDD simulations (solid lines show the best power-law fit for each initial dislocation density); and (b) the magnitude of the power-law exponent, $|n|$, vs. initial dislocation density as computed from 3-D DDD simulations, alongside those computed from the current experiments and those published in the literature [13,14,22].

dislocation length in the microcrystal. The mean length can be computed from the stochastics of dislocation source lengths as a function of initial dislocation density, as postulated in Ref. [23]. At low dislocation densities the flow strength is governed by the resolved shear strength necessary to activate the weakest links in the crystal (e.g. for $D = 1$ μm and at $\rho = 10^{12}$ m^{-2}, we get $\lambda = 0.2$ μm, $\tau_{source} = 95$ MPa, $\tau_{forest} = 9.5$ MPa and $\tau = 104.5$ MPa). As the dislocation density increases, the probability of finding weaker dislocation sources increases and the microcrystal softens (e.g. for $D = 1$ μm and at $\rho = 10^{13}$ m^{-2}, we get $\lambda = 0.36$ μm, $\tau_{source} = 53$ MPa, $\tau_{forest} = 30$ MPa and $\tau = 83$ MPa). The limiting case is when the strength of the weakest link ($\tau_{source} \propto 1/(D/2)$) is on the order of the strength required to overcome the dislocation forest ($\tau_{forest} \propto \sqrt{\rho}$). At this limiting case the microcrystal strength would be independent of size, and would be entirely governed by the forest hardening mechanism and thus deform in a bulk-like manner.

Figure 4(b) shows the magnitude of the power-law exponent, $|n|$, vs. the initial dislocation density as evaluated from DDD simulations and experiments. Unlike DDD simulations, the exact initial dislocation densities in the microcrystals after micromachining are unknown experimentally. Thus, the experimental data are plotted as a function of the initial dislocation density of the parent crystals they were fabricated into. A good agreement is observed between the DDD predictions and experiments. The size-scaling power-law exponent is observed to be proportional to the initial dislocation density following the relationship: $|n| \propto \rho_0^{-0.18}$.

In summary, bulk [1 1 0] Ni single crystals were pre-strained into stage III up to 23% strain. Microcrystals with various sizes and th esame [1 1 0] orientation were FIB milled into the pre-strained crystal and redeformed in compression. The effect of the initial heterogeneous dislocation structure and the high dislocation density on the strength scaling was then analyzed. This study complements previous studies [7,6,15,13] by examining the effect of dislocation density on microcrystal response through pre-straining of a bulk fcc crystal to obtain a high residual dislocation density composed of a heterogeneous dislocation cell structure. From our experiments and DDD simulations we have shown that increasing the initial dislocation density results in decreasing the power-law exponent governing the strength-scaling relationship of Ni single crystals. The experimental results also show that microcrystals with diameters $D \geqslant 5$ μm deform at lower flow strengths than the strength reached at the end of pre-straining of the parent bulk crystal. This may be attributed to the process of artificially selecting only a sub-region of the dislocation forest and bounding this region with free surfaces, giving the evolving dislocations new pathways to defeat the forest at yield. Finally, the extent of the effect of the initial dislocation density on size-dependent strengthening can be explained in terms of the strength of the weakest links in the microcrystal vs. the strength required to overcome the dislocation forest.

Support from the U.S. Air Force Research Laboratory (AFRL), Materials and Manufacturing Directorate, and by computer resources grant from the DoD High-Performance Computing Modernization Program at the AFRL-DoD Supercomputing Research Center (AFRL-DSRC).

[1] M.D. Uchic, D.M. Dimiduk, J.N. Florando, W.D. Nix, Mater. Res. Soc. Symp. Proc. 753 (2003) BB1.4.
[2] M.D. Uchic, D.M. Dimiduk, J.N. Florando, W.D. Nix, Science 305 (2004) 986.
[3] M.D. Uchic, P.A. Shade, D.M. Dimiduk, Annu. Rev. Mater. Res. 39 (2009) 361.
[4] J.R. Greer, J.Th.M. De Hosson, Prog. Mater. Sci. 56 (2011) 654.
[5] H. Bei, S. Shim, E.P. George, M.K. Miller, E.G. Herbert, G.M. Pharr, Scripta Mater. 57 (2007) 397.
[6] H. Bei, S. Shim, G.M. Pharr, E.P. George, Acta Mater. 56 (2008) 4762.
[7] S. -W Lee, S.M. Han, W.D. Nix, Acta Mater. 57 (2009) 4404.
[8] A.S. Schneider, B.G. Clark, C.P. Frick, P.A. Gruber, E. Arzt, Philos. Mag. Lett. 90 (2010) 841.
[9] S.I. Rao, D.M. Dimiduk, T.A. Parthasarathy, M.D. Uchic, M. Tang, C. Woodward, Acta Mater. 56 (2008) 3245.
[10] E.G. Popkova, A.A. Predvodi, Sov. Phys. Crystllogr. 18 (1974) 647.
[11] E. Springer, Z. Metallk. 62 (1971) 298.
[12] V.A. Starenchenko, D.V. Lychagin, R.V. Shaekhov, É.V. Kozlov, Russ. Phys. J. 42 (1999) 653.
[13] D.M. Dimiduk, M.D. Uchic, T.A. Parthasarathy, Acta Mater. 53 (2005) 4065.
[14] C.P. Frick, B.G. Clark, S. Orso, A.S. Schneider, E. Arzt, Mater. Sci. Eng. A 489 (2008) 319.
[15] P.S. Phani, K.E. Johanns, G. Duscher, A. Gali, E.P. George, G.M. Pharr, Acta Mater. 59 (2011) 2172.
[16] J.G. Sevillano, I.O. Arizcorreta, L.P. Kubin, Mater. Sci. Eng. A (2001) 393.
[17] S.I. Rao et al., Unpublished work, 2012.
[18] H. Mughrabi, Phys. Status Solidi A 104 (1987) 107.
[19] Y.S. Choi, M.D. Uchic, T.A. Parthasarathy, D.M. Dimiduk, Scripta Mater. 57 (2007) 849.
[20] J.A. El-Awady, S.B. Biner, N.M. Ghoniem, J. Mech. Phys. Solids 56 (2008) 2019.
[21] J.A. El-Awady, M. Wen, N.M. Ghoniem, J. Mech. Phys. Solids 57 (2009) 32.
[22] A.S. Schneider, D. Kiener, C.M. Yakacki, H.J. Maier, P.A. Gruber, N. Tamura, M. Kunz, A.M. Minor, C.P. Frick, Mater. Sci. Eng. A 559 (2012) 147.
[23] T.A. Parthasarathy, S.I. Rao, D.M. Dimiduk, M.D. Uchic, D.R. Trinkle, Scripta Mater. 56 (2007) 313.